Effect of sliding friction on gear noise based on a refined vibro-acoustic formulation

Song He[a], Rajendra Singh[b] and Goran Pavić[c]

(Received: 3 January 2008; Revised: 5 May 2008; Accepted: 5 May 2008)

An improved source-path-receiver model of a single mesh geared system is developed and validated to quantify the effect of sliding friction between gear teeth on the structure-borne whine noise. The source sub-system of a spur gear pair predicts interfacial bearing forces in the line-of-action and off line-of-action directions for two whine excitations (static transmission error and sliding friction). Next, a finite element model of the gearbox with embedded bearing stiffness matrices is developed to characterize the structural paths and to calculate the surface velocity distributions. Predictions are first validated by comparing with structural modal tests and transfer function measurements from gear mesh to the housing plates. Radiated noise is then estimated by using two approximate methods, namely the Rayleigh integral method and a substitute source technique. The overall vibro-acoustic model is validated by comparing radiated sound pressure calculations with measured noise data over a range of operating torques. The proposed formulation provides an efficient analytical and computational tool to quantify the relative contribution of sliding friction to the structure-borne noise, which is found to be significant when the transmission error is minimized say via tooth modifications. ***© 2008 Institute of Noise Control Engineering.***

Primary subject classification: 11.1.3; Secondary subject classification: 75

1 INTRODUCTION

Most gear noise researchers[1–3] have assumed that the static transmission error (STE) is the main source of whine (steady state noise at gear mesh frequencies and side-bands). Consequently, transmission errors are minimized in a methodical manner via tooth modifications. However, high precision gears are still noisy in many applications. One plausible explanation is that the sliding friction becomes a potential noise source, especially in spur gears at certain torques or tribological conditions[4–7]. Accordingly, we consider two concurrent excitations, namely the unloaded static transmission error and sliding friction, to a geared system, as shown in Fig. 1. Objectives of this article are: (1) Develop a refined source-path-receiver model that characterizes the structural paths in two directions; also, propose analytical and efficient computational tools to predict noise radiated from the gearbox panels. (2) Quantify the relative contributions of transmission error versus sliding friction noise to the overall whine noise, and validate predictions of the structural transfer functions and sound pressure with measurements for one example case (NASA gearbox with spur gears).

2 LITERATURE REVIEW AND PROBLEM FORMULATION

The literature on the vibro-acoustic models of the entire geared system[2,3,8] is rather sparse. For the internal geared system, only a few investigators have incorporated the torsional and translational motions in both line-of-action (LOA) and off line-of-action (OLOA) directions[4–7] although many lumped parameter models have been developed over the last four decades[1–3]. The vibration transmission path through bearings has been well described by the stiffness matrix that was analytically formulated by Lim and Singh[9]. Rook and Singh[10] analyzed the gearbox using the mobility synthesis method and derived a procedure of calculating narrowband vibratory power flows, which recognizes rolling

[a] Acoustics and Dynamics Laboratory, The Ohio State University, 201 West 19th Avenue, Columbus OH 43210 USA; email: he.81@osu.edu

[b] Acoustics and Dynamics Laboratory, The Ohio State University, 201 West 19th Avenue, Columbus OH 43210 USA; email: singh.3@osu.edu

[c] Laboratoire Vibrations Acoustique, Institut National des Sciences Appliquées de Lyon, Bâtiment Saint-Exupéry, 25 bis, avenue Jean Capelle, F-69621 Villeurbanne Cedex FRANCE; email: goran.pavic@insa-lyon.fr

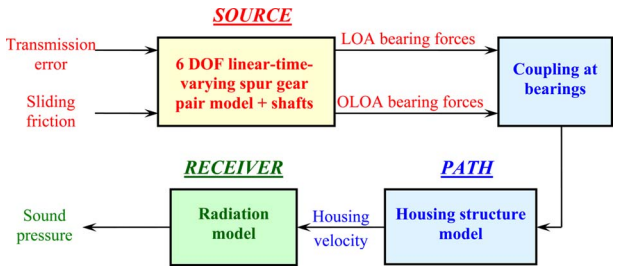

Fig. 1—Vibro-acoustic model of a simplified geared system with two excitations at the gear mesh, structure-borne paths through bearings and then radiation from the gearbox. Here, LOA is the line-of-action and OLOA is the off-line-of-action.

element bearings as a multi-dimensional compliant and dissipative connection. Moreover, the vibration behavior of the gearbox housings has been examined by using finite element analysis (FEA)[11,12], experimental modal analysis[13] and statistical energy analysis (SEA)[14] methods. For instance, Lim and Singh[11] developed a finite element model of flexible casing to predict bearing and mount transmissibilities in a simple geared system. Van Roosmalen[12] reported that the natural frequencies from a finite element analysis correlated well with modal tests for a simple gearbox at lower frequencies. Lim and Singh[14] developed a two sub-system SEA model which included an analytical description of the coupling loss factor associated with the vibration transmission through rolling element bearings.

To predict sound radiation from the gearbox, prior researchers have relied on either simple radiation efficiency models or large scale numerical codes (such as the boundary elements). However, a combination of finite and boundary element models often requires extensive computational time while yielding minimal insight. Jacobson et al.[15] predicted the radiation efficiency of a gearbox plate using ideal radiators like monopole, dipole, cylinder and the like but achieved limited success when compared with in-situ radiation measurements. Such simplified models yield only global trends and do not adequately describe the modal radiation characteristics of a gearbox. Kartik and Houser[16] proposed a semi-empirical frequency-response based model to predict noise radiation from gearbox housings with a multi-mesh gear set. Also, they utilized the broad-band radiation efficiency model of a rectangular plate; again their model yields only broad trend over a range of gear mesh frequencies. Recently, Singh et al.[17] developed a semi-empirical model for predictions of the radiated whine noise by combining a linear time-invariant model of the internal geared system with measured vibro-acoustic transfer functions of the structural paths (from gear/pinion motions in two directions to the radiated sound). They also found that the friction force dictates the OLOA dynamics and it significantly influences the maximum force in the LOA direction. Overall, the above mentioned studies do not provide a tractable analytical or computational vibro-acoustic system model and all have included only the transmission error as the source except Singh et al.[17] who included sliding friction as well. We propose to overcome this deficiency in our article though we focus on a single mesh spur gear set in a simple gearbox.

In our formulation (as conceptually shown in Fig. 1), the pinion and gear of the internal spur gear pair sub-system are modeled as rigid disks, and the elastic deformations of the shaft and bearings are modeled using lumped elements. Vibratory angular motions are small in comparison to the mean motion, and the mean load is assumed to be high such that the dynamic load is not sufficient to cause tooth separations[18]; this leads to a linear time-varying system formulation. Though both excitations are interrelated, they are assumed to be most dominant in LOA and OLOA directions, respectively. Hence, only corresponding structural paths in these two directions are considered by neglecting the moment transfer elements in the bearing stiffness matrices. Also, by assuming the housing mass is much larger than the gears and shafts, an impedance mismatch is created with a rigid boundary condition at the bearing location[2]. Thus, the internal geared system could be modeled separately and its resulting forced response provides force excitations to the structural paths. Further, we analytically or numerically describe the entire system model, unlike Kartik and Houser[16] or Singh et al.[17], who included empirical transfer functions. Finally, for the sake of illustration, we apply our formulation to the NASA test facility gearbox[13] and it is assumed that the top plate is the main radiator due to its relatively high mobility as well as the way it is constructed.

3 SOURCE SUB-SYSTEM MODEL WITH TWO EXCITATIONS

The source sub-system is described by a recently developed 6DOF, linear time-varying spur gear pair model[19] that incorporates the sliding friction and realistic mesh stiffness, which is calculated by an accurate finite element/contact mechanical code[20]. Rigid bearings are assumed as boundary conditions due to the impedance mismatch at the interface of shafts and bearings. Overall, the system formulations are summarized as follows. The governing equations for the torsional motions $\theta_p(t)$ and $\theta_g(t)$ of pinion and gear are:

$$J_p\ddot{\theta}_p(t) = T_p + \sum_{i=0}^{n} X_{pi}(t)F_{pfi}(t) - \sum_{i=0}^{n} r_{bp}N_{pi}(t) \quad (1)$$

$$J_g\ddot{\theta}_g(t) = -T_g + \sum_{i=0}^{n} X_{gi}(t)F_{gfi}(t) + \sum_{i=0}^{n} r_{bg}N_{gi}(t) \quad (2)$$

where $n=\text{floor}(\sigma)$ in which the "floor" function rounds off the contact ratio σ to the nearest integer (towards a lower value); J_p and J_g are the polar moments of inertia of the pinion and gear; T_p and T_g are the external and braking torques; r_{bp} and r_{bg} are base radii of the pinion and gear; and, $N_{pi}(t)$ and $N_{gi}(t)$ are the normal loads defined as follows:

$$N_{pi}(t) = N_{gi}(t) = k_i(t)[r_{bp}\theta_p(t) - r_{bg}\theta_g(t) + x_p(t) - x_g(t)] + c_i(t)[r_{bp}\dot{\theta}_p(t) - r_{bg}\dot{\theta}_g(t) + \dot{x}_p(t) - \dot{x}_g(t)] \quad (3)$$

where $k_i(t)$ and $c_i(t)$ are the realistic mesh stiffness and viscous damping profiles; $x_p(t)$ and $x_g(t)$ denote the LOA displacements of pinion and gear centers. The sliding friction forces $F_{pfi}(t)$ and $F_{gfi}(t)$ as well as their moment arms $X_{pi}(t)$ and $X_{gi}(t)$ of the i^{th} meshing pair are derived as:

$$F_{pfi}(t) = \mu_i(t)N_{pi}(t), \quad (4a)$$

$$F_{gfi}(t) = \mu_i(t)N_{gi}(t) \quad (4b)$$

$$X_{pi}(t) = L_{XA} + (n-i)\lambda + \text{mod}(\Omega_p r_{bp}t, \lambda), \quad (5a)$$

$$X_{gi}(t) = L_{YC} + i\lambda - \text{mod}(\Omega_g r_{bg}t, \lambda) \quad (5b)$$

where the sliding friction is formulated by $\mu_i(t) = \mu_0\text{sgn}[\text{mod}(\Omega_p r_{bp}t, \lambda) + (n-i)\lambda - L_{AP}]$; λ is the base pitch; "sgn" is the sign function; the modulus function $\text{mod}(x,y) = x - y\cdot\text{floor}(x/y)$, if $y \neq 0$; Ω_p and Ω_g are the nominal speeds (in rad/s); and, L_{AP}, L_{XA} and L_{YC} are geometric length constants[19]. The governing equations for $x_p(t)$ and $x_g(t)$ motions in the LOA direction are:

$$m_p\ddot{x}_p(t) + 2\zeta_{pSx}\sqrt{K_{pSx}m_p}\dot{x}_p(t) + K_{pSx}x_p(t) + \sum_{i=0}^{n} N_{pi}(t) = 0 \quad (6)$$

$$m_g\ddot{x}_g(t) + 2\zeta_{gSx}\sqrt{K_{gSx}m_g}\dot{x}_g(t) + K_{gSx}x_g(t) + \sum_{i=0}^{n} N_{gi}(t) = 0 \quad (7)$$

Here, m_p and m_g are the masses of the pinion and gear; K_{pSx} and K_{gSx} are the effective shaft stiffness values in the LOA direction, and ζ_{pSx} and ζ_{gSx} are the damping ratios. Likewise, the translational motions $y_p(t)$ and $y_g(t)$ in the OLOA direction are governed by:

$$m_p\ddot{y}_p(t) + 2\zeta_{pSy}\sqrt{K_{pSy}m_p}\dot{y}_p(t) + K_{pSy}y_p(t) - \sum_{i=0}^{n} F_{pfi}(t) = 0 \quad (8)$$

$$m_g\ddot{y}_g(t) + 2\zeta_{gSy}\sqrt{K_{gSy}m_g}\dot{y}_g(t) + K_{gSy}y_g(t) - \sum_{i=0}^{n} F_{gfi}(t) = 0 \quad (9)$$

Finally, the dynamic forces at the bearings are as:

$$F_{pBx}(t) = -K_{pSx}x_p(t) - 2\zeta_{pSx}\sqrt{K_{pSx}m_p}\dot{x}_p(t), \quad (10a)$$

$$F_{pBy}(t) = -K_{pSy}y_p(t) - 2\zeta_{pSy}\sqrt{K_{pSy}m_p}\dot{y}_p(t), \quad (10b)$$

$$F_{gBx}(t) = -K_{gSx}x_g(t) - 2\zeta_{gSx}\sqrt{K_{gSx}m_g}\dot{x}_g(t), \quad (11a)$$

$$F_{gBy}(t) = -K_{gSy}y_g(t) - 2\zeta_{gSy}\sqrt{K_{gSy}m_g}\dot{y}_g(t). \quad (11b)$$

Both LOA and OLOA bearing forces are predicted for the example case (unity-ratio NASA spur gear pair with tip relief) with parameters of the pinion/gear given as follows[19]: number of teeth=28; outside diameter=3.738 in; root diameter=3.139 in; diametral pitch=8 in^{-1}; center distance=3.5 in; pressure angle=20°; face width=0.25 in; tooth thickness=0.191 in; and elastic modulus=30×10^6 psi. Predictions are then converted from time domain into frequency domain by using the fast Fourier transform (FFT) analysis method; comparisons at the first three gear mesh frequencies are given in Fig. 2 over a range of the pinion torque T_p. Observe that the friction dominated OLOA dynamic responses are less sensitive to a variation in T_p. Dynamic interactions between the sliding friction and profile modifications (embedded in the effective mesh stiffness k) may be analyzed in future work[21].

4 STRUCTURAL PATHS AND CONTRIBUTION FROM SLIDING FRICTION

4.1 Bearing and Housing Models

Predicted bearing forces by the source sub-system provide excitations to the multi-input, multi-output (MIMO) structural paths for the gearbox of Fig. 3(a). Force excitations are coupled at each bearing via a stiffness matrix $[K]_{Bm}$ (of dimension 5) that is calculated by using the algorithm proposed by Lim and Singh[9]. Nominal shaft loads and bearing preloads are assumed

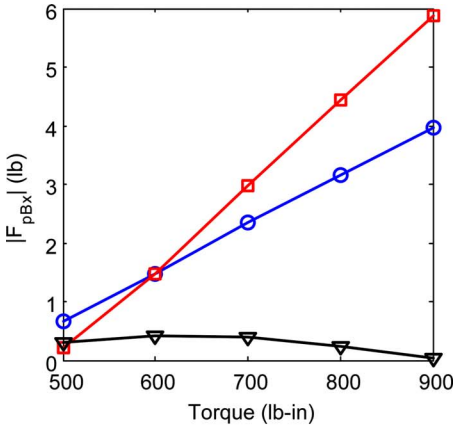

(a)

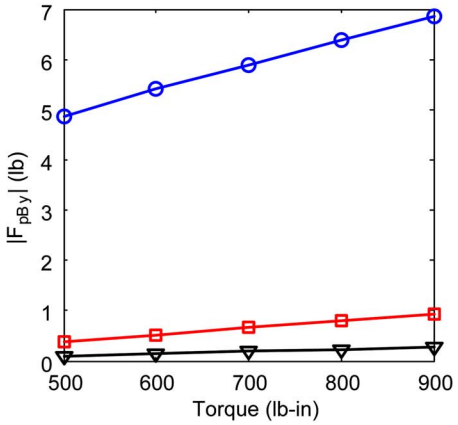

(b)

Fig. 2—Dynamic bearing forces predicted under a range of T_p given Ω_p=4875 RPM and 140 °F. (a): LOA bearing force; (b) OLOA bearing force. Key: m is the gear mesh frequency index. Key: ⊖, m=1; ⊟, m=2; ▽, m=3.

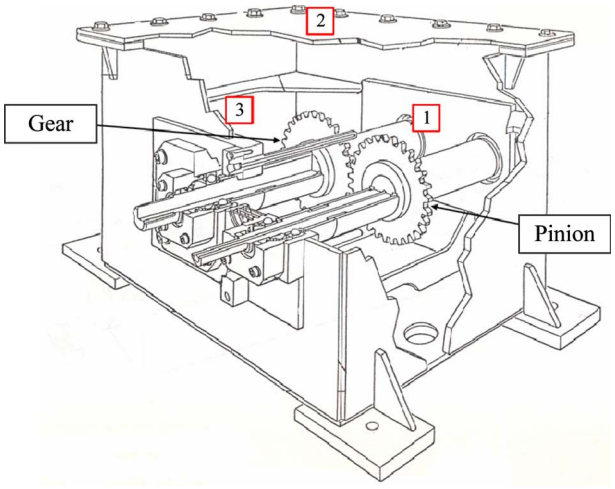

(a)

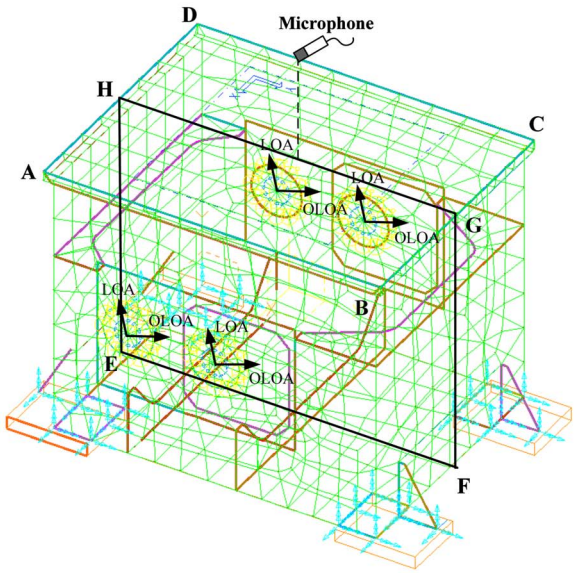

(b)

Fig. 3—(a) Schematic of the NASA gearbox; (b) Finite element model of the NASA gearbox with embedded bearing stiffness matrices.

to ensure a time-invariant $[K]_{Bm}$. In order to focus on the transmission error and sliding friction paths in the LOA and OLOA directions respectively, $[K]_{Bm}$ is intentionally reduced into a 2 by 2 matrix by neglecting the moment transfer terms[10] and assuming that no axial force is generated by the spur gear sub-system. Calculated nominal bearing stiffness elements[9] are $K_{Bx}=K_{By}=2.8\times10^6$ lb/in at the mean operating condition; these are much larger than the shaft stiffness of 1.29×10^5 lb/in. This confirms the impedance mismatch assumption made regarding the shaft/bearing interface.

The implementation of $[K]_{Bm}$ into the finite element gearbox model of Fig. 3(b) requires special attention[11,22]. At high excitation (mesh) frequencies (say up to 5 kHz), the geometric dimensions of the bearings are comparable to the plate flexural wavelength. Hence the holes may significantly alter the plate dynamics and such effects must be modeled[22]. A rigid (with Young's modulus 100 times the casing steel) and massless beam element (with density 1% of the casing steel) is used to model the interface from shaft to the bearings. Only a small beam is selected in order to ensure that none of the beam resonances is found in the frequency range of interest. The shaft (beam) element is connected to the central bearing node though orthogonal foundation stiffness elements (K_{Bx} and K_{By}) in the LOA and OLOA directions, respectively. The central node is then connected to the circumferential bearing nodes by 12 rigid and massless beams (one at each rolling element's angular position) which form a "star" configuration, such that the

Table 1—Comparison of measured natural frequencies and finite element predictions of the NASA gearbox[24].

Gearbox mode index	Measurements[24] (Hz)	Finite element predictions (Hz)
1	658	650
2	1049	988
3	1709	1859
4	2000	1940
5	2276	2328
6	2536	2566
7	2722	2762
8	2962	2962

displacement of the plate around the bearing hole are equal to the "housing node" at the center.

4.2 Experimental Studies and Validation of Structural Model

The finite element model of Fig. 3 is created by using I-DEAS[23] for the NASA gearbox with bearing holes, embedded stiffness matrices $[K]_{Bm}$, stiffening plates as well as clamped boundary conditions at four rigid mounts. Although the internal sub-system with gear pair and shafts is not included, it has been shown[11] that an "empty" gearbox tends to describe the global dynamics of the entire system. Table 1 confirms that the natural frequencies predicted by the finite element model correlate well with measurements reported by Oswald et al.[24] despite minor structural modifications made to the gearbox. Mode shape predictions also match well with modal tests; Fig. 4 gives a typical comparison of structural mode at the 8th natural frequency (f_n=2962 Hz).

In order to validate the structural paths, several transfer functions were measured for the NASA gearbox by assuming that the quasi-static system response is similar to the response under non-resonant rotating conditions. The gearbox was modified to allow controlled excitations to be applied to the gear-mesh and measured[25]. Brackets were welded to the bedplate of the gear-rig to mount shakers in the LOA and OLOA directions outside the gearbox, as shown in Fig. 5(a). Stinger rods were connected from the shakers through two small holes in the gearbox and attached to a collar on the input shaft. Two mini accelerometers were fastened to a block behind the loaded gear tooth to measure the LOA and OLOA mesh accelerations. Band-limited random noise signals were then used as excitation signals and tests were done with only one shaker activated at a time with a 600 lb-in static preload (design load for the gears). Dynamic responses were measured to generate vibro-acoustic transfer functions. Sensor # 1 of Fig. 5(a) is a tri-axial accelerometer mounted on the output shaft bearing cap to measure the LOA, OLOA, and axial vibrations. Sensors #2 and #3 are unidirectional accelerometers mounted on the top and back plates, respectively.

The transfer function of the combined source-path sub-systems is predicted as:

$$\tilde{H}_{S-P}(\omega) = \tilde{H}_S(\omega) \cdot \tilde{H}_P(\omega) = \tilde{H}_S(\omega) \cdot \frac{\tilde{Y}_{plate}(\omega)}{\tilde{Y}_{bearing}(\omega)} \tag{12a}$$

$$\tilde{Y}_{plate}(\omega) = \frac{\tilde{V}_{plate}(\omega)}{\tilde{F}_{bearing}(\omega)}, \tag{12b}$$

$$\tilde{Y}_{bearing}(\omega) = \frac{\tilde{V}_{bearing}(\omega)}{\tilde{F}_{bearing}(\omega)} \tag{12c}$$

where $\tilde{Y}_{plate}(\omega)$ and $\tilde{Y}_{bearing}(\omega)$ are the transfer and driving point mobilities for the (top) plate and the bearing; these are derived from the finite element model of the gearbox by using the modal expansion method with 1% structural damping for all modes. Further, $\tilde{H}_S(\omega)$ is the motion transmissibility from gear mesh to translational bearing responses (in LOA or OLOA direction) by using the 8DOF linear time-invariant spur gear model[17,25]. Note that such a lumped model is insufficient to capture the bending and flexural modes of the gear blanks and shafts. Figure 5(b) shows that the measured motion transmissibility (OLOA direction) from gear mesh to the bearing compares well with predicted $|\tilde{H}_S(\omega)|$ based on the linear time-invariant model[25]. In Fig. 5(c), the predicted motion transmissibility $|\tilde{H}_{S-P}(\omega)|$ from gear mesh to the top plate correlates reasonably well with measurement given the complexity of the system. The highest frequency is chosen such that the shortest wave-length is 4 times larger than the model element dimension on the top plate. Recall that interactions between the shaft and bearings/casing were neglected in our model by imposing the impedance mismatch condition. Consequently, an empirical weighting function $20\log_{10}|\tilde{W}(\omega)| = 10$ dB is added (uniformly over the entire frequency range) to "tune" the $|\tilde{H}_P(\omega)|$ prediction in Fig. 5(c) for better comparison. Further work is needed to quantify this effect; Karthik and Houser[16] had also noted this issue.

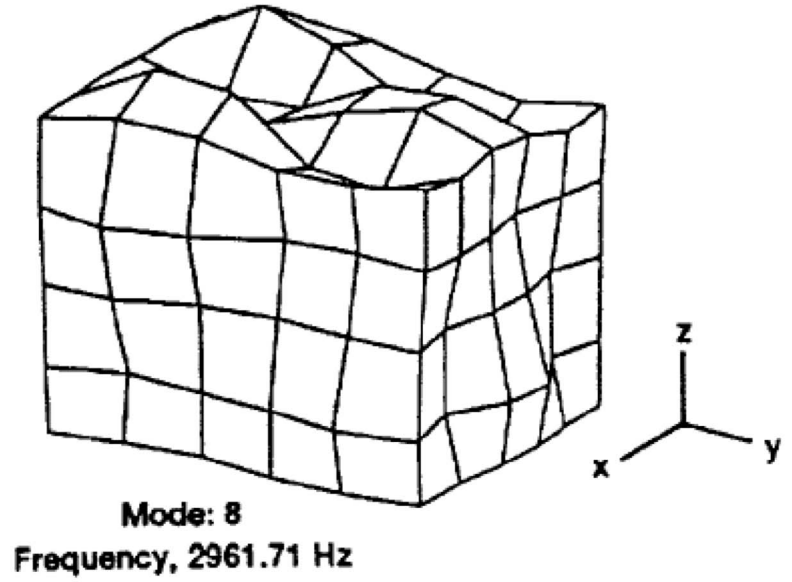

(a)

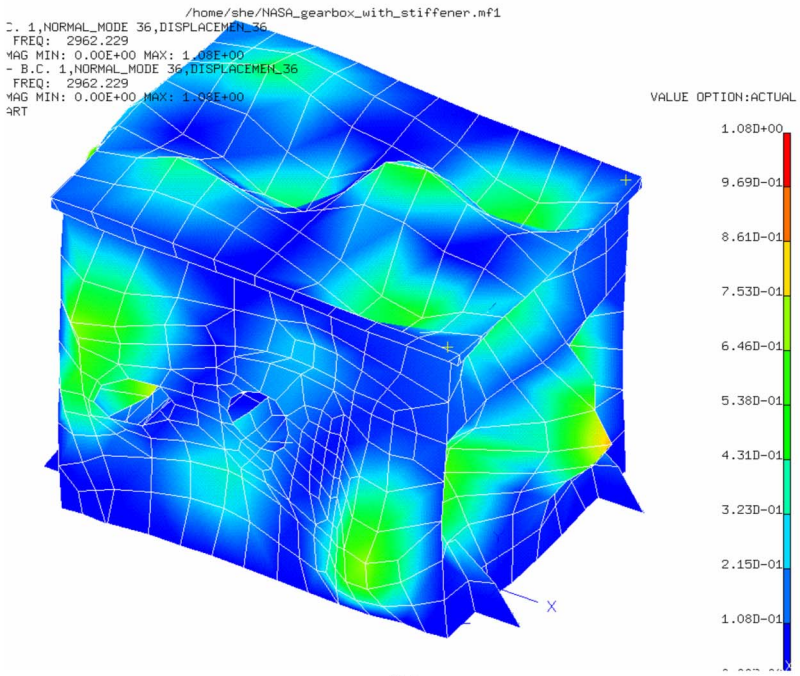

(b)

Fig. 4—Comparison of one elastic deformation mode of the gearbox (at 2962 Hz*): (a) modal experiment result*[24]*; (b) finite element prediction.*

4.3 Comparison of Structural Paths in LOA and OLOA Directions

First, assume that (i) the bearing forces predicted by the source model[19] are in phase at either bearing end for the pinion (or gear) shaft; (ii) the bearing forces of pinion and gear are same in magnitude but opposite in directions due to the symmetry of unity ratio gear pair. Second, the overall structural paths are derived for the transmission error controlled LOA (or x) path and the friction dominated OLOA (or y) path in terms of the combined (effective) transfer mobilities $\tilde{Y}_{e,x}(\omega)$ and $\tilde{Y}_{e,y}(\omega)$:

$$\tilde{Y}_{e,x}(\omega) = \sum_n \tilde{W}_{p,x,n}\tilde{Y}_{p,x,n}(\omega) - \sum_n \tilde{W}_{g,x,n}\tilde{Y}_{g,x,n}(\omega) \tag{13a}$$

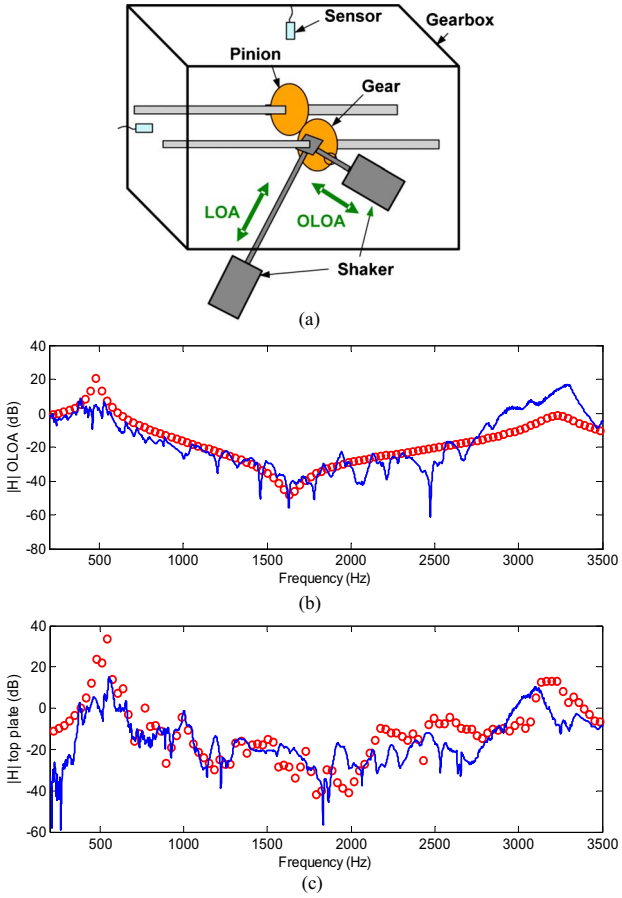

Fig. 5—(a) Experiment used to measure the structural transfer functions; (b) Comparison of the transfer function magnitudes from gear mesh to bearings; (c) Comparison of the transfer function magnitudes from gear mesh to a sensor on the top plate (gearbox). Key: —, measurements; ∘, predictions, —.

$$\tilde{Y}_{e,y}(\omega) = \sum_n \tilde{W}_{p,y,n}\tilde{Y}_{p,y,n}(\omega) - \sum_n \tilde{W}_{g,y,n}\tilde{Y}_{g,y,n}(\omega) \tag{13b}$$

where $\tilde{W}$ is the empirical weighting function (10 dB applied over the spectrum); and the subscript n is the index of the two ends of pinion/gear shafts. Figure 6 compares the magnitudes of $\tilde{Y}_{e,x}(\omega)$ and $\tilde{Y}_{e,y}(\omega)$ at the sensor location on the top plate. Different peaks are observed in the LOA and OLOA paths spectra. This implies that at certain frequencies (e.g. 650 and 1700 Hz), the OLOA path (and thus the frictional effects) could be dominant over the LOA path (and thus the transmission error effects) given comparable force excitation levels. The proposed method thus provides an efficient tool to quantify and evaluate the relative contribution of structural path due to sliding friction.

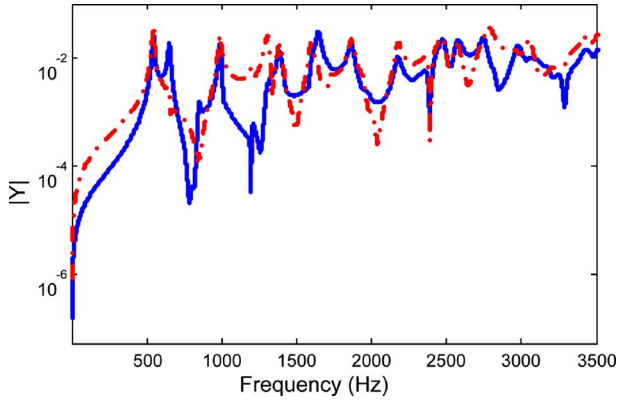

Fig. 6—Magnitudes of the structural path mobilities in the OLOA and LOA directions. Response for each (due to excitation at the gear mesh) is calculated at the sensor location on the top plate (gearbox). Key: —, mobility of the OLOA path; -·-·, mobility of the LOA path.

The top plate velocity distribution $\tilde{V}_{top}(\omega)$ could then be predicted by using Eqn. (14), where $\tilde{F}_{p,B,x}(\omega)$ and $\tilde{F}_{p,B,y}(\omega)$ are the pinion bearing forces predicted by the source model in the LOA and OLOA directions. Figure 7(a) shows the surface interpolated velocity distributions on the top plate, as define below, at three mesh harmonics ($m=1,2,3$) given $T_p=500$ lb-in and $\Omega_p=4875$ RPM:

$$\tilde{V}_{top}(\omega) = \frac{1}{2}\tilde{F}_{p,B,x}(\omega)\tilde{Y}_{e,x}(\omega) + \frac{1}{2}\tilde{F}_{p,B,y}(\omega)\tilde{Y}_{e,y}(\omega) \tag{14}$$

5 PREDICTION OF RADIATED NOISE AND CONTRIBUTION FROM SLIDING FRICTION SOURCE

5.1 Sound Pressure Prediction Using Rayleigh Integral Technique

Since the rectangular top plate is the main radiator[24] of the gearbox due to its relatively high mobility, Rayleigh integral[26] is used to approximate the sound pressure by assuming that the top plate is placed in an infinite rigid baffle and each elementary plate surface is an equivalent point source in a rigid wall. The sound pressure amplitude at frequency ω (rad/s) is given as follows where ρ is the air density, $\tilde{Q}_i(\omega)=\tilde{V}_i(\omega)\Delta S_i$ is the source strength of i^{th} equivalent point source with area ΔS_i, $k(\omega)$ is the wave number and r_i is the distance from the i^{th} source to the receiver:

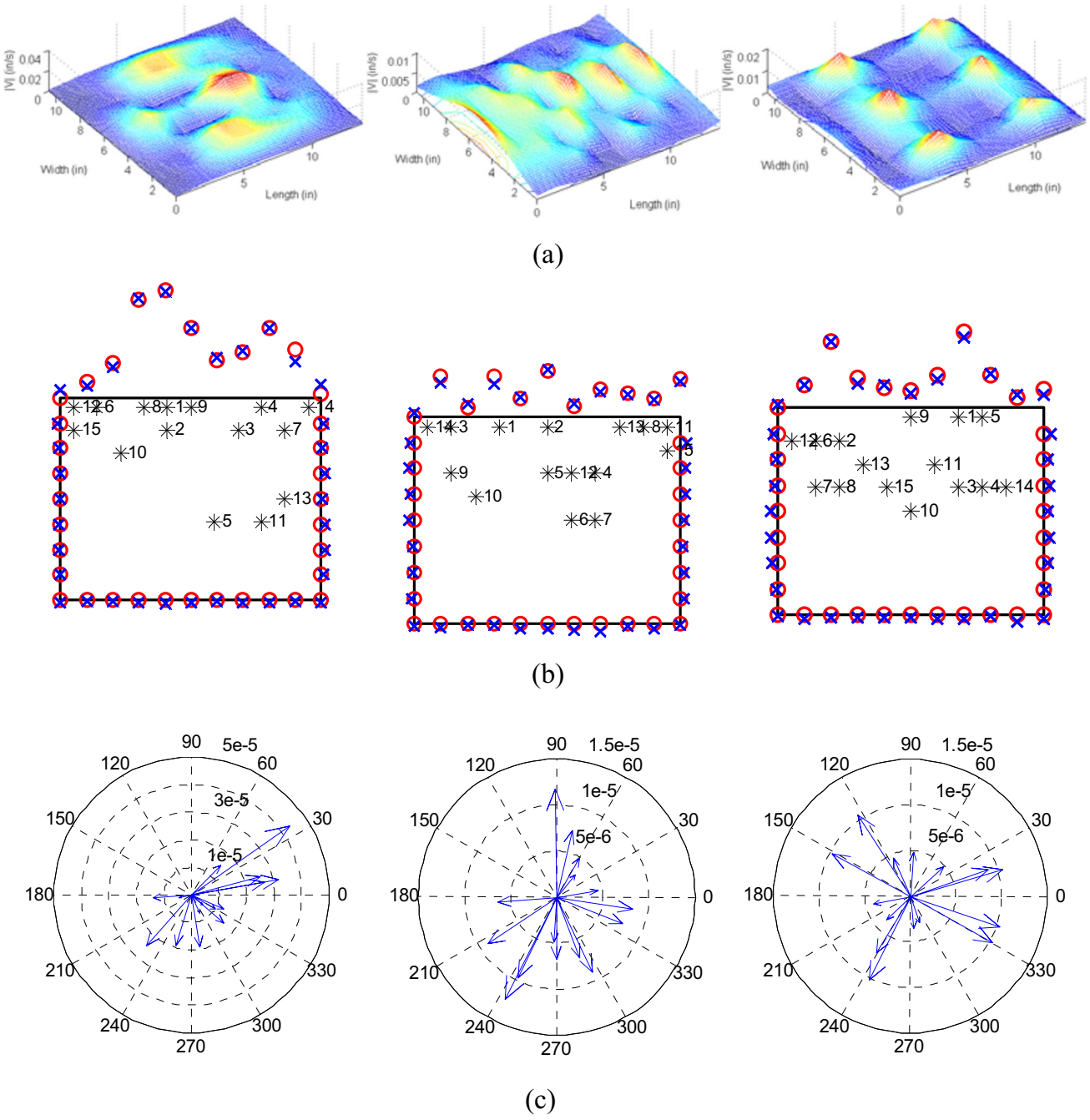

Fig. 7—Comparison of the normal surface velocity magnitudes and substitute source strength vectors under T_p=500 lb-in and Ω_p=4875 RPM. (a) Line 1: interpolated surface velocity on top plate; (b) Line 2: simplified 2D gearbox model with 15 substitute source points; Key: ∘, original surface velocity magnitude; ×, surface velocity magnitude by substitute sources; ∗, locations of substitute sources. (c) Line 3: substitute source strengths in complex plane for 2D gearbox. Column 1: gear mesh frequency index m=1; Column 2: m=2; Column 3: m=3.

$$\tilde{P}(\omega) = \frac{j\omega\rho}{2\pi} \sum_i \frac{\tilde{Q}_i(\omega)}{r_i} e^{-jk(\omega)r_i} \qquad (15)$$

For the calculation of whine noise, ω is chosen to coincide with first three gear mesh frequencies of interest; ΔS_i is chosen such that its dimension (on the top plate) is smaller than 1/4 of the wave-length at the highest gear mesh frequency. The overall noise is then calculated by combining the contributions of all equivalent sources (using Eqn. (15)) at the receiver. Compared with conventional boundary element analysis, Rayleigh integral approximates sound pressure in a fraction of the computation time[26]. Hence, it is more suitable for parametric design studies. Although some

researchers[27] have pointed out that Rayleigh integral may give large errors for sound pressure prediction if applied to strongly directional, three dimensional (3D) fields, such errors are not significant in our application due to a flat top plate and favorable surroundings (such as rigid side plates and the anechoic chamber).

5.2 Sound Pressure Prediction Using Substitute Source Method

As an alternative to the Rayleigh integral technique or the boundary element method, a newly developed algorithm based on the substitute source approach[28] is used to compute the radiated or diffracted sound field. It is conducted by removing the gearbox and introducing acoustic sources within the liberated space which yield the desired boundary conditions at the box surface (Neumann problem). Solutions are obtained in terms of the locations and/or the strengths of the substitute sources by minimizing the error function between original and estimated particle velocity normal to the interface surface[28].

Since the surface velocity distributions on the gearbox plate(s) are essentially symmetric along the center lines due to geometric symmetry, velocity distributions in Fig. 3(b) along the border lines of EFGH plane are chosen to simplify the 3D gearbox into a 2D radiation model for simpler data representation as well as faster computation. Zero (negligible) velocity distribution is assumed along lines EF, FG and HE since the microphone (receiver) is positioned above the center of major radiator, i.e. the top plate. A 2D line source uniformly pulsating with unit-length volume velocity Q' is chosen as the substitute source. Its radiation field is the same in any plane perpendicular to the source line. Amplitudes of the sound pressure ($\tilde{P}$) and radial velocity ($\tilde{V}_r$) of such source are given by the following, where $H_v^{(2)}$ is the Hankel function of second kind and order v.

$$\tilde{P}(\omega) = \frac{k(\omega)\rho c}{4}\tilde{Q}'(\omega)H_0^{(2)}[k(\omega)r], \qquad (16a)$$

$$\tilde{V}_r(\omega) = -j\frac{k(\omega)}{4}\tilde{Q}'H_1^{(2)}[k(\omega)r] \qquad (16b)$$

A "greedy search" algorithm is used to search for "optimal" substitute sources: First, a large number of candidate source positions within the vibrating body are defined, e.g. at the vertices of a square grid. Second, a single position is first found which allows the point source to produce the smallest possible deviation between the original and estimated normal surface velocities. The estimation is then subtracted from the original velocity to get a velocity residual. Third, among the rest of candidate points, a new position is found which makes the second source maximally reduce the velocity residual of the first step. Once found, the source strengths of both sources are adjusted for a best fit of the original surface velocity and a new residual velocity. Each subsequent step defines a new optimum source position among the ones not already used[28]. The source strengths are curve-fit by minimizing the root-mean-square (RMS) value of the velocity error. The vector of complex-valued source strength $\underline{\tilde{Q}}'$ is related (as shown below) to the vector $\underline{\tilde{V}}_n$ of complex-valued normal surface velocity at control points via the source-velocity transfer matrix $\tilde{T}$ where $r_{ij}=|\vec{r}_i-\vec{r}_j|$ and α_{ij} is the angle between vector $\vec{r}_i-\vec{r}$ and the outer normal to the surface.

$$\underline{\tilde{Q}}'(\omega) = \underline{\underline{\tilde{T}}}^{-1}(\omega)\underline{\tilde{V}}_n(\omega), \qquad (17a)$$

$$\tilde{T}_{ij}(\omega) = -j\frac{k(\omega)}{4}H_1^{(2)}[k(\omega)r_{ij}]\cos(\alpha_{ij}) \qquad (17b)$$

To minimize the impact of an ill-conditioned matrix, the number of control points is kept well above that of independent source points. Minimization of the RMS error using pseudo-inverse yields the following, where the asterisk signifies the conjugate transpose:

$$\underline{\tilde{Q}}'(\omega) = [\underline{\underline{\tilde{T}}}(\omega)^*\underline{\underline{\tilde{T}}}(\omega)]^{-1}\underline{\underline{\tilde{T}}}(\omega)^*\underline{\tilde{V}}_n(\omega) \qquad (18)$$

The difference between synthesized and original surface normal velocities is:

$$\Delta\underline{\tilde{V}}(\omega) = \underline{\underline{\tilde{\Xi}}}(\omega)\underline{\tilde{V}}_n(\omega), \qquad (19a)$$

$$\underline{\underline{\tilde{\Xi}}}(\omega) = \underline{\underline{\tilde{T}}}(\omega)[\underline{\underline{\tilde{T}}}(\omega)^*\underline{\underline{\tilde{T}}}(\omega)]^{-1}\underline{\underline{\tilde{T}}}(\omega)^* - \underline{\underline{\tilde{I}}}(\omega) \qquad (19b)$$

where $\underline{\underline{\tilde{I}}}(\omega)$ is the identity matrix. The matrix $\underline{\underline{\tilde{\Xi}}}(\omega)$ appears as a velocity error matrix. The RMS velocity error is normalized by using the RMS value of original velocity as:

$$\tilde{e}_{RMS}(\omega) = \frac{\tilde{E}_{RMS}(\omega)}{\tilde{V}_{n,RMS}(\omega)} = \sqrt{\frac{\underline{\tilde{V}}_n(\omega)^*\underline{\underline{\tilde{\Xi}}}(\omega)^*\underline{\underline{\tilde{\Xi}}}(\omega)\underline{\tilde{V}}_n(\omega)}{\underline{\tilde{V}}_n(\omega)^*\underline{\tilde{V}}_n(\omega)}} \qquad (20)$$

This search algorithm described[28] is based on engineering "common sense" rather than a rigorous mathematical optimization of the substitute source positions. Consequently, it may not necessarily lead to optimum positioning, i.e. to the solution which gives the smallest possible RMS velocity error. The overall advantage is in its simplicity of application as well as in providing solutions that are much better than those obtained via an arbitrary selection of the source

positions. Note that the substitute source technique as elaborated above could be applied to solve other radiation problems. This also permits an evaluation of the acoustic source properties.

5.3 Noise Prediction vs. Measurements

Figure 7(a) shows predictions of surface interpolated velocity distribution on the top plate at the first three mesh harmonics under T_p=500 lb-in and Ω_p =4875 RPM. Note that predictions at higher frequencies (e.g. mesh index m=3) are less "reliable" due to the limitation of element dimensions as compared the wave length. The symmetry of surface velocity distribution leads to the simplification into a 2D gearbox model of Fig. 7(b). To ensure necessary accuracy for acoustic radiation, selected (central) lines of the 2D plane should capture the dominant structural modes of Fig. 7(a). Also, the structural wavelength along the central line should be higher than the acoustic wavelength of interest to ensure the validity of the 2D approach.

The source points of Fig. 7(b) are chosen from a mesh grid of candidate points not too close to the boundary to prevent a generation of steep gradients in surface pressure. Observe that only 15 substitute sources tend to predict well the surface distribution of velocity magnitude at the gear mesh harmonics. Figure 7(c) illustrates the predicted source strengths of the substitute sources (in the complex plane) for evaluation of the acoustic source properties. A single dominant substitute source is observed at the first mesh harmonic (monopole-like acoustic source); however, several dominant substitute sources are present and these are more equally distributed in the complex plane at higher harmonics (multi-pole acoustic sources).

A simplification from 3D into 2D gearbox model requires an examination of the surface (structural) modes and a careful selection of representative plane, which poses additional limitations to its application as a more "universal" method. However, once applicable, the substitute source method provides several benefits. First, it enables an efficient evaluation of the acoustic source characteristics for whine noise. Second, unlike the Rayleigh integral technique which assumes that the top plate is placed in an infinite rigid baffle, it takes the body shape into account and thus reduces the errors especially in the lower frequency range. This also allows a straight forward synthesis of the radiation field for all sources by using a simple superposition as long as diffraction from the sources does not take place. Finally, compared with boundary element analysis, it does not suffer from the problems of singularities or

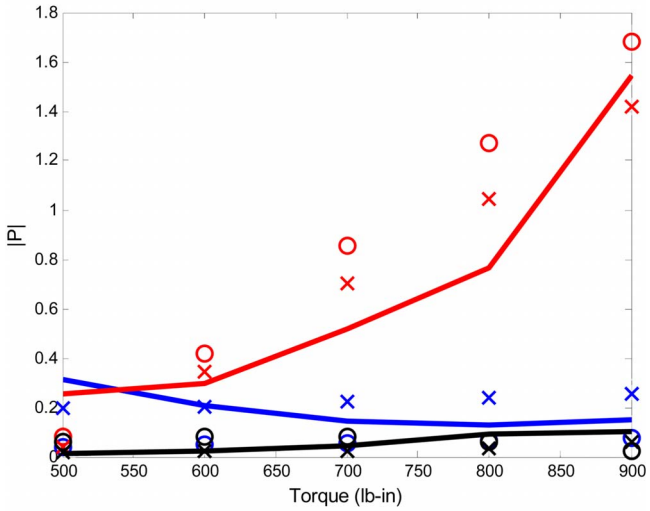

Fig. 8—Sound pressures (Pa) at the first three gear mesh frequencies (with speed Ω_p =4875 RPM) over a range of torque T_p at 140 °F. *Key: —, measurements (6″ above the top plate); ∘, Rayleigh integral predictions; ×, substitute source predictions. Color code: Blue, gear mesh frequency index m=1; red, m=2; black, m=3.*

uniqueness of solution. Nonetheless, it is an engineering (approximate) method and must be judiciously applied.

Figure 8 compares the sound pressure measured at the microphone 6 inch above the top plate to predictions by using both the Rayleigh integral as well as the substitute source methods over a range of pinion torque given Ω_p=4875 RPM and 140 °F. Finally, it is worthwhile to notice that the second mesh harmonic, which is most susceptible to the sliding friction, becomes increasingly more dominant at higher torques for our example case.

6 CONCLUSION

A refined source-path-receiver model has been developed which characterizes the sliding friction induced structural path and associated noise radiation. Proposed Rayleigh integral method and substitute source technique are capable of calculating the acoustic field and quantifying the frictional noise. For instance, Fig. 9 compares the sound pressure level predicted given Ω_p=4875 RPM and 140 °F under T_p =500 lb-in (close to the "optimal" load where transmission error is minimized) and under high torque with T_p=800 lb-in. At each gear mesh frequency, individual contributions of transmission error (via the LOA path) and frictional effects (via the OLOA path) are compared to the overall whine noise. Observe in Fig.

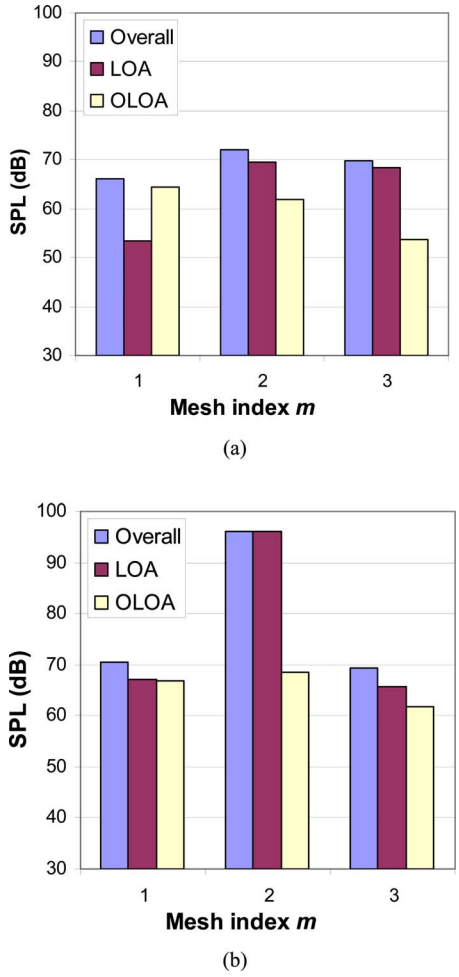

Fig. 9—Overall sound pressure levels (dB re 2e-5 Pa) and their contributions predicted at 6″ above the top plate under Ω_p=4875 RPM *and* 140 °F. *(a) Mean load* T_p=500 lb-in *(optimal load for minimum transmission error); (b) mean load* T_p=800 lb-in.

9(a) that near the "optimal" load, sliding friction induced noise is comparable to the transmission error induced noise (especially for the first two mesh harmonics); thus sliding friction should be considered as a significant contributor to the whine noise. However, at "non-optimal" torques in Fig. 9(b), friction induced noise is overwhelmed by the transmission error noise, thus sliding friction could be negligible under such conditions. This confirms that the sliding friction should be viewed as a potential contributor to structure-borne noise for high precision, high power density geared systems.

Despite the complexity of the geared system and many assumptions made during the modeling process (such as neglecting the moment transfer elements at the bearings and a simplification of the 3D gearbox into 2D problem), predictions correlate well with measurements in terms of trends and relative magnitudes at first three gear mesh harmonics. This result suggests a promising start to the substitute source technique. Further work is needed to extend the substitute source method and its variants (such as multi-pole sources[29]) in predicting the noise from a more complicated gearbox in 3D space, as well to quantify the acoustic source strengths and directivity. As part of the ongoing work, the approximate sound radiation methods will be compared with the boundary-element techqiue[30] which could also be applied to the problem.

7 ACKNOWLEDGEMENTS

We gratefully acknowledge the Marie Curie Fellowship of the European Commission for financially supporting this research. V. Asnani and F. Oswald of the NASA Glenn Research Center are thanked for conducting the experiments. We acknowledge Dr. T. Rook of Goodrich Co. and Dr. R. Gunda of Advanced Numerical Solutions Inc. for their comments and suggestions. Dr. T. Lim from the University of Cincinnati is thanked for providing the bearing stiffness software.

8 REFERENCES

1. H. N. Ozguven and D. R. Houser, "Mathematical models used in gear dynamics - a review", *J. Sound Vib.*, **121**, 383–411, (1988).
2. G. Steyer, "Influence of gear train dynamics on gear noise", *NOISE-CON 87 Proc.*, 53–58, (1987).
3. A. Parey and N. Tandon, "Spur gear dynamic models including defects: A review", *Shock Vib. Dig.* **35**(6), 465–478, (2003).
4. P. Velex and V. Cahouet, "Experimental and numerical investigations on the influence of tooth friction in spur and helical gear dynamics", *ASME J. Mech. Des.*, **12** (4), 515–522, (2000).
5. O. Lundvall, N. Strömberg and A. Klarbring, "A flexible multi-body approach for frictional contact in spur gears", *J. Sound Vib.* **278**(3), 479–499, (2004).
6. D. R. Houser, M. Vaishya and J. D. Sorenson, "Vibro-acoustic effects of friction in gears: An experimental investigation", *SAE*, Paper #2001- 01-1516, (2001).
7. J. Borner and D. R. Houser, "Friction and bending moments as gear noise excitations", *SAE*, Paper #961816, (1996).
8. T. C. Lim and R. Singh, "A review of gear housing dynamics and acoustics literature", *NASA Tech. Memo.*, 89-C-009, (1989).
9. T. C. Lim and R. Singh, "Vibration transmission through rolling element bearings. Part I: Bearing stiffness formulation", *J. Sound Vib.* **139**(2), 179–199, (1990).
10. T. E. Rook and R. Singh, "Mobility analysis of structure-borne noise power flow through bearing in gearbox-like structures", *Noise Control Eng. J.*, **44**(2), 69–78, (1996).
11. T. C. Lim and R. Singh, "Vibration transmission through rolling element bearings. Part II: System studies", *J. Sound Vib.* **139**(2), 201–225, (1990).
12. A. Van Roosmalen, "Design tools for low noise gear transmissions", Ph.D. Dissertation, Eindhoven University of Technology, 76-100, (1994).
13. F. K. Choy, Y. F. Ruan, J. J. Zakrajsek and F. B. Oswald, "Modal simulation of gearbox vibration with experimental correlation", NASA-TM-105702, (1992).
14. T. C. Lim and R. Singh, "Statistical energy analysis of a gearbox with emphasis on the bearing path", *Noise Control Eng. J.*,

37(2), 63–69, (1991).
15. M. F. Jacobson, R. Singh and F. B. Oswald, "Acoustic radiation efficiency models of a simple gearbox", *ASME Design Eng. Conf.* DE 88, 597–601, (1996).
16. V. Kartik and D. R. Houser, "An investigation of shaft dynamic effects on gear vibration and noise excitation", *SAE Trans.*, **112**, 1737–1746, (2003).
17. R. Singh, A. Lake, V. Asnani and S. He, "Vibro-acoustic model of a geared system including friction excitation", *INTER-NOISE 2007*, Paper #663296, 28–31 Aug, Istanbul, TURKEY, (2007).
18. G. W. Blankenship and A. Kahraman, "Steady state forced response of a mechanical oscillator with combined parametric excitation and clearance type non-linearity", *J. Sound Vib.* **185**(5), 743–765, (1995).
19. S. He, R. Gunda and R. Singh, "Effect of sliding friction on the dynamics of spur gear pair with realistic time-varying stiffness", *J. Sound Vib.* **301**, 927–949, (2007).
20. External2D (CALYX software), A contact mechanics/finite element (CM/FE) tool for spur gear design, ANSOL Inc. ⟨www.ansol.com ⟩, Hilliard, OH, (2002).
21. S. He and R. Singh, "Dynamic interactions between sliding friction and tip relief in spur gears", *10th Int. Power Trans. and Gearing Conf.*, Paper #DETC 2007-34077, Las Vegas, NE, (2007).
22. T. E. Rook and R. Singh, "Structural intensity calculations for compliant plate-beam structures connected by bearings", *J. Sound Vib.*, **211**(3), 365–388, (1998).
23. I-DEAS, Online tutorials, SDRC Inc., Milford, MI, (1998).
24. F. B. Oswald, A. F. Seybert, T. W. Wu and W. Atherton, "Comparison of analysis and experiment for gearbox noise", NASA-TM-105330, (1992).
25. R. Singh, "Dynamic analysis of sliding friction in rotorcraft geared systems," Technical report submitted to the Army Research Office, Grant number DAAD19-02-1-0334, (2005).
26. L. Cremer and M. Heckl, *Sound Radiation from Structures*, Chapter 6 on "Structure-borne Sound," Springer-Verlag, New York, (1973).
27. D. W. Herrin, F. Martinus, T. W. Wu and A. F. Seybert, "A new look at the high frequency boundary element and Rayleigh integral approximations", *SAE*, Paper #03NVC-114, (2003).
28. G. Pavić, "An engineering technique for the computation of sound radiation by vibrating bodies using substitute sources", *Acta Acust.*, **91**, 1–16, (2005).
29. G. Pavić, "A technique for the computation of sound radiation by vibrating bodies using multipole substitute sources", *Acta Acust. (Beijing)*, **92**, 112–126, (2006).
30. R. Gunda and S. Vijayakar, "Application of the Fast Multipole Method (FMM) for acoustic analysis", *NOISE-CON 2007*, Paper #196, 22-24 Oct., Reno, NE, (2007).